Supporting Information to

Using Carbon Nanodots as Inexpensive and Environmentally Friendly Sensitizers in Mesoscopic Solar Cells

Experimental and Computational Details

Carbon nanodot synthesis: CNDs were synthesized in a domestic microwave using citric acid (CA), urea (U), and formic acid (FA) as precursors and water as solvent. Different optical properties could be obtained by varying the molar ratios of the precursors. In this work, we used **CND1** (CA:U:FA 1:1:2) and **CND2** (CA:U:FA 1:1:20). Precursor solutions were reacted for 5 min. The product was re-dispersed in water, centrifuged to remove any insoluble components and finally dried in an oven.

Solar cell fabrication and characterization: Fluorine-doped tin oxide (FTO) substrates were sonicated for 15 min with a detergent solution, washed with deionized water, and again sonicated in isopropyl alcohol for 15 min. FTO glass plates were immersed into a 40 mM aqueous $TiCl_4$ solution at 70 °C for 30 min and washed with water and ethanol. Treated substrates were sintered at 450 °C for 30 min. The nanocrystalline TiO_2 layers (WER2-O, Dyesol) were prepared on FTO glass plates by using a doctor blade technique and pre-dried at 125 °C for 6 min. The TiO_2 anodes were gradually heated under air flow to 325 °C and held for 5 min, further heated to 375 °C and held for 5 min, heated to 450 °C and held for 30 min, and finally sintered at 500 °C for 15 min. For alpha-step thickness measurements, we used a Dektak XT profilometer from Bruker. The average thickness of the films was 12 µm. The thickness did not change after sensitization, even after 24 h in pH 1 solutions. Therefore, we conclude that the morphology of the layers was similar for every cell (see also Fig. S10). The anodes were pH-dependently sensitized for different times in aqueous CND solutions (1 mg/mL). For preparation of the counter-electrodes two holes (0.1 mm) were drilled into FTOs via sandblasting prior to the cleaning procedure (*vide supra*). FTOs were coated with a thin film of chloroplatinic solution (4.88 mM) in isopropyl alcohol. Thereby, always the same amount of chloroplatinic solution (26 µL) was used to assure the same coverage of the FTO. Then, the slides were annealed to 390 °C for 15 min. Counter-electrodes were freshly prepared for every measurement to assure reproducible results.

The photoanodes and the counter-electrodes were assembled into a sealed sandwich-type cell by heating at 130 °C with a controlled pressure using a hot-melt ionomer film (Surlyn, Solaronix). The I^-/I_3^- electrolyte contained 0.04 mol/L I_2, 0.10 mol/L guanidinium thiocyanate, 0.6 mol/L 1-butyl-3-methylimidazolium iodide, 0.5 mol/L 4-*tert*-butylpyridine in an acetonitrile/valeronitrile mixture (85:15 v/v). The electrolyte was introduced via capillary forces. Finally, the two holes were sealed using an additional Surlyn and a cover glass.

The photocurrent measurements were performed using a 150 W lamp (Xenon lamp, calibrated to 1000 W m^{-2} under AM 1.5 conditions with a Si-Reference cell (Oriel SRC-1000-TC-K-KG5-N). Currentvoltage measurements were measured by using a potentiostat/galvanostat (PGSTAT30N, Autolab equipped with a frequency response analyzer module – FRA) in the range of -0.8 to 0.2 V.

For fabrication of TiO_2 films for spectroscopy, a special highly transparent paste was used for (TiO_2 HT/SP, Solaronix). The treatment of the TiO_2 layer was identical to the treatment of FTOs for solar cells. The anodes were sensitized for 6 h at pH from 7 to 1.

Photovoltage transients were taken with the use of a pump pulse generated by a blue ($\lambda_{max} \approx 490$ nm, Luxeon LXHL-BB01) light emitting diode (LED) controlled by a fast solid-state switch (Metrohm PGSTAT30N with a short-interval sampling module (Dynload interface) for pulsed light measurements). The time resolved voltage measurements were recorded using the Nova ver. 1.11.2 software. For the photovoltage decay measurements, the cell was illuminated to reach a steady voltage. In detail, the cell was allowed to reach steady-state conditions without illumination the cells for 10 sec under potentiostatic conditions (i.e. V = 0, short-circuit). Afterwards, the cell was illuminated with the blue LED and switched to galvanostatic conditions (i.e. I = 0, open-circuit) for 20 sec to reach photostationary equilibrium conditions. The LED was then switched off and the decay of the photovoltage was recorded.

Spectroscopic details: Steady-state absorption measurements were carried out with a Lambda 2 UV/Vis/NIR-spectrometer from Perkin Elmer. Steady-state fluorescence emission measurements were performed with a FluoroMax-3 fluorometer from Horiba Jobin Yvon. All spectra were corrected for the instrument response. Time-Correlated Single-Photon Counting measurements were recorded with a FluoroLog-3 lifetime spectro-fluorometer (Horiba) supplied with an integrated TCSPC software. Sample excitation was achieved with a 403 nm laser diode from HORIBA. Femtosecond transient absorption studies were carried out using a transient absorption pump/probe system (TAPPS) with an amplified titanium:sapphire CPA-2101 laser (775 nm output, 1 kHz repetition rate, 150 fs pulse width) from CLARK-MXR INC. Excitation wavelength of 480 nm was realized with a non-collinear optical parametric amplifier (NOPA).

Analytical Ultracentrifugation: A preparative centrifuge, type Optima L-90K from Beckman Coulter, modified with a multiwavelength detector was used for the sedimentation velocity experiments. Detailed information regarding the hardware as well as the data acquisition software is available in literature.[1,2] Two-sector titanium centerpieces from Nanolytics, Germany, with a path length of 12 mm were used for the SV-experiments. Data was acquired every ten minutes at 55,000 rpm for 30 h, 25 °C and a radial resolution of 50 µm. Water with 50 mM NaCl was used as a solvent. Multiwavelength intensity data were recorded and converted to absorbance data. Data at a wavelength of 431 nm were used for hydrodynamic analyses. Data evaluation was carried out using the software Ultrascan3 and the 2-dimensional spectrum analysis (2DSA) as well as the parametrically constrained spectrum analysis (PCSA).[3,4] 2DSA was used to fit the samples' menisci and to calculate the time and radius invariant noise vectors. However, peak splitting occurred in the final pseudo 3-dimensional distributions derived by 2DSA and Monte Carlo analyses due to the pronounced polydispersity of both samples. The origin of peak splitting is currently under investigation and will be presented elsewhere. Therefore, we used PCSA in combination with Tikhonov regularization (PCSA-TR) to derive the final *s-D* distributions. Different parametrisations were compared for the PCSA and the increasing sigmoid variant was finally chosen because it provided by far the lowest root mean square deviation (RMSD). For 2DSA and PCSA the partial specific volume (inverse of the particle's density) was fitted as a function of the sedimentation coefficient while keeping the frictional ratio constant ($f/f_0 = 1$).

Computational details: Quantum mechanical Born-Oppenheimer molecular-dynamics simulations were performed with EMPIRE14.[5] We used the semiempirical AM1 Hamiltonian in the unrestricted Hartree-Fock formalism.[6] The instantaneous temperature was controlled via a Berendsen thermostat with a relaxation time of 100 fs.[7] The simulations were equilibrated for 1200 fs, followed by a 3600 fs production run.

Analytical Ultracentrifugation

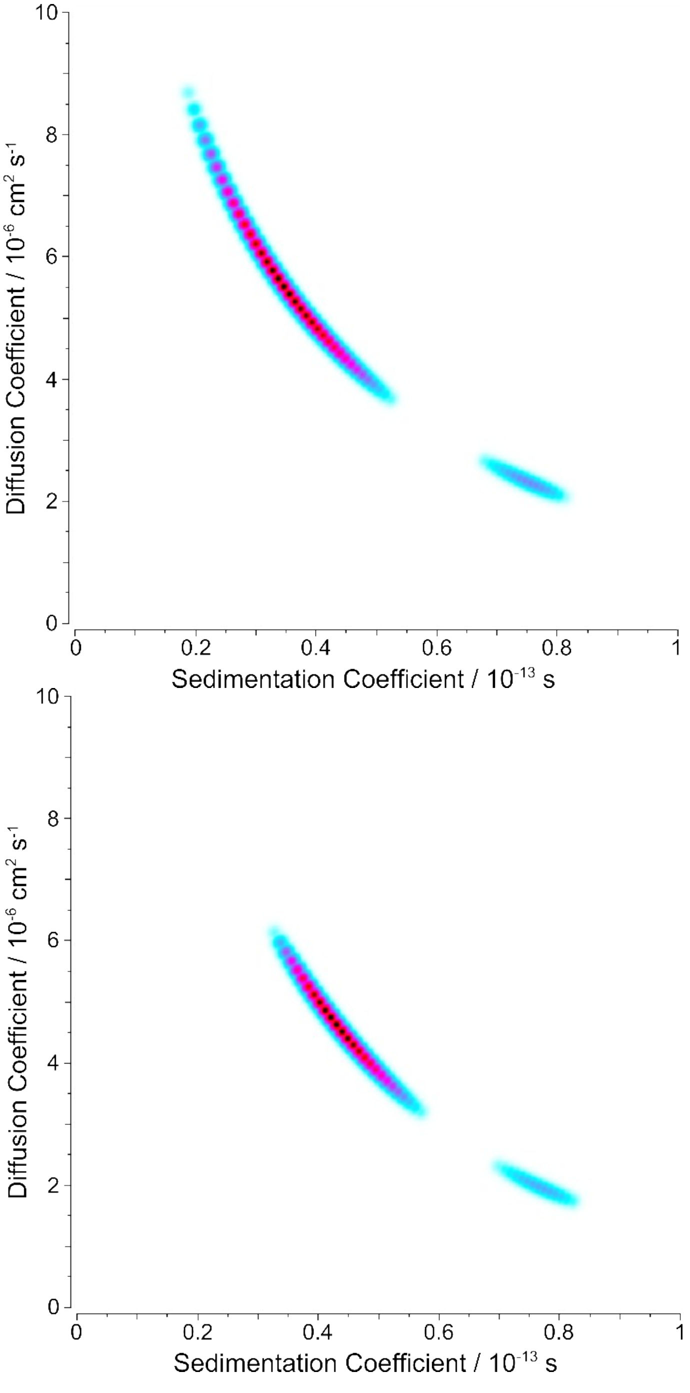

Fig. S1. Pseudo 3-dimensional plots of the CND1 (top) and CND2 (down) clearly showing their polydispersity in s and D. Values are given for standard conditions for water at 20 °C. Higher concentration is indicated by a more reddish color.

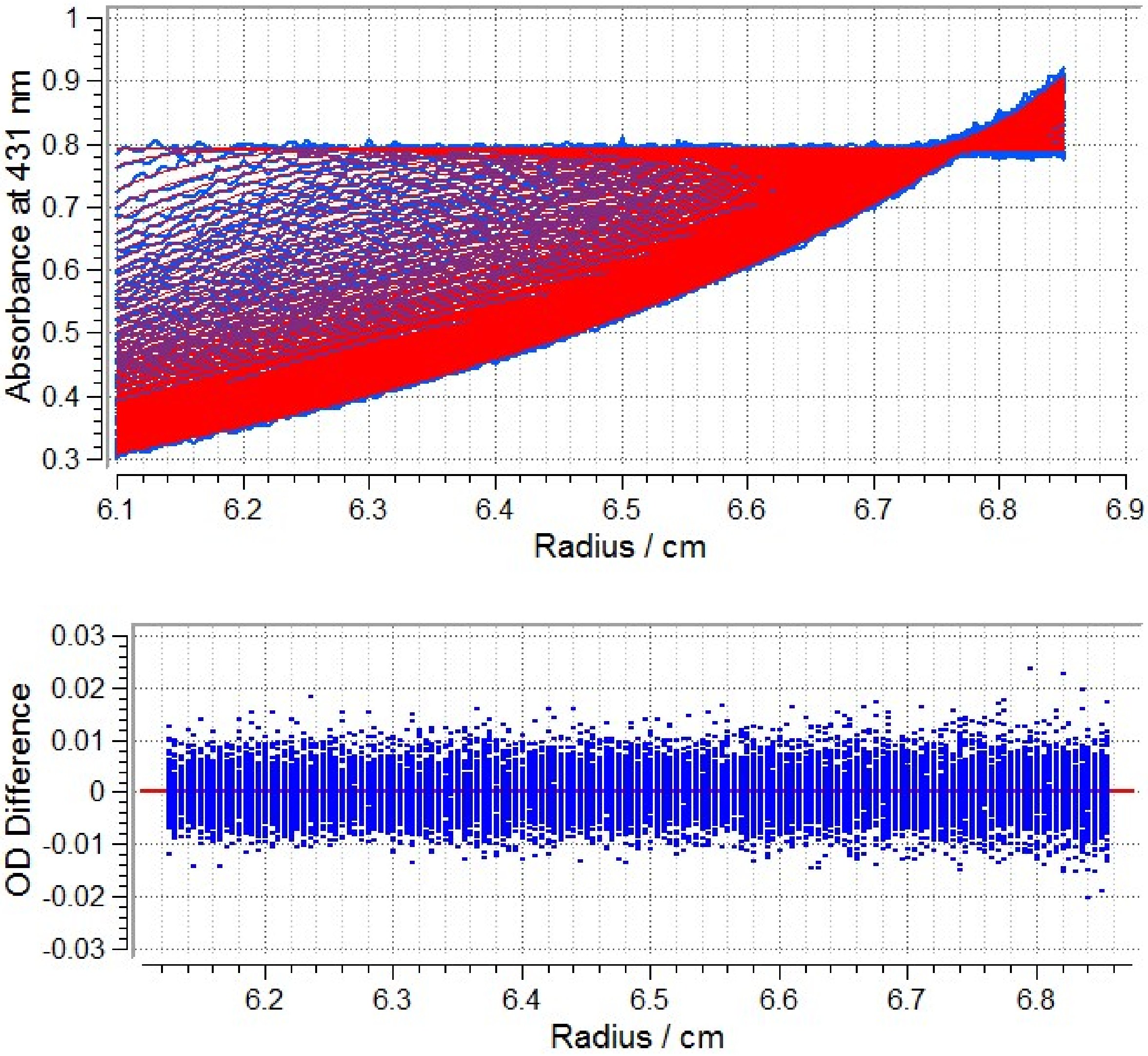

Fig. S2: Top: Experimental (blue) and fit (red) data of CND1. Residuals data as obtained for the PCSA-TR analyses with a RMSD of 0.0048 OD.

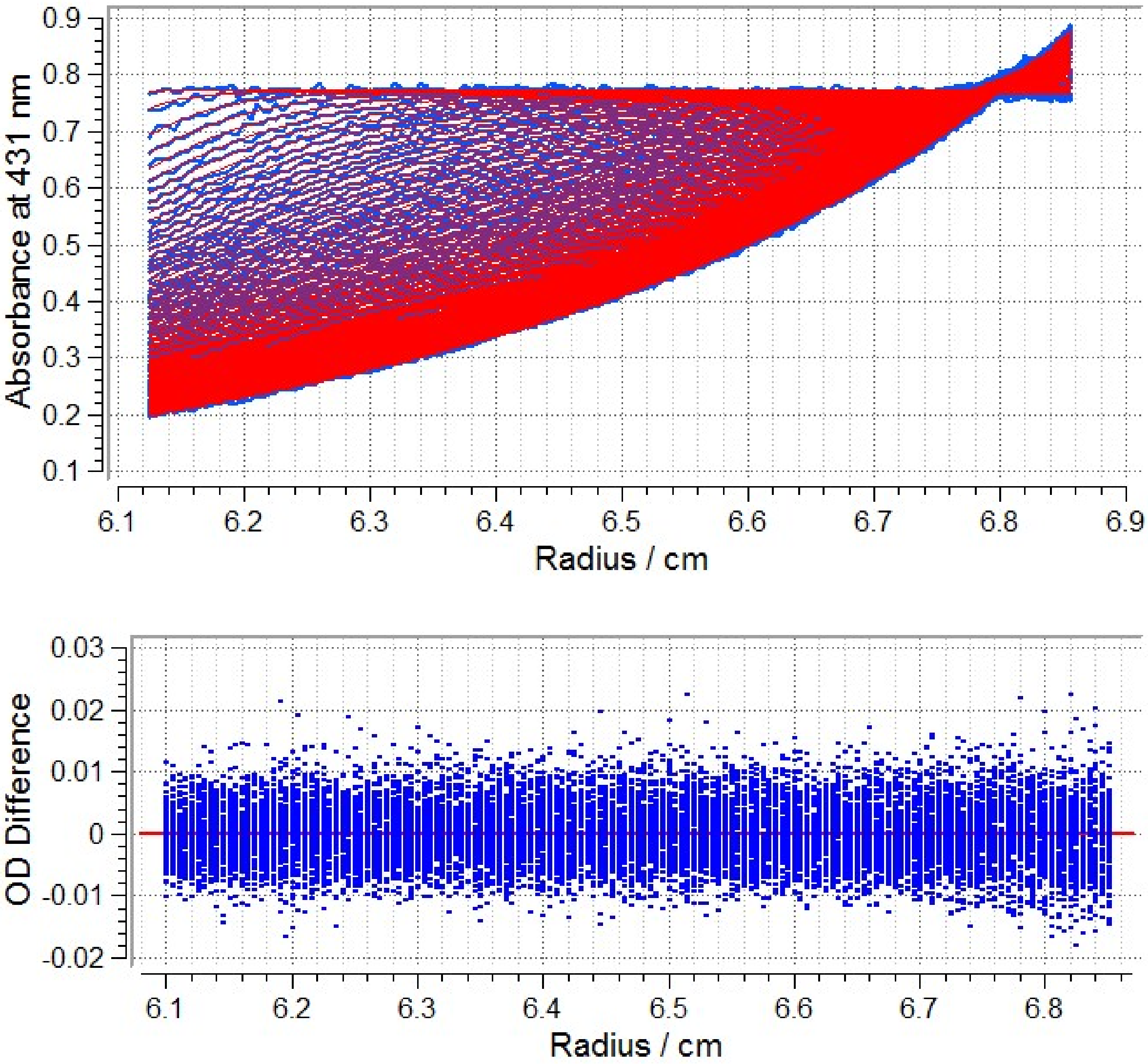

Fig. S3: Top: Experimental (blue) and fit (red) data of the CND2. Residuals data as obtained for the PCSA-TR analyses with a RMSD of 0.0046 OD.

2D-Excitation-Emission Spectra

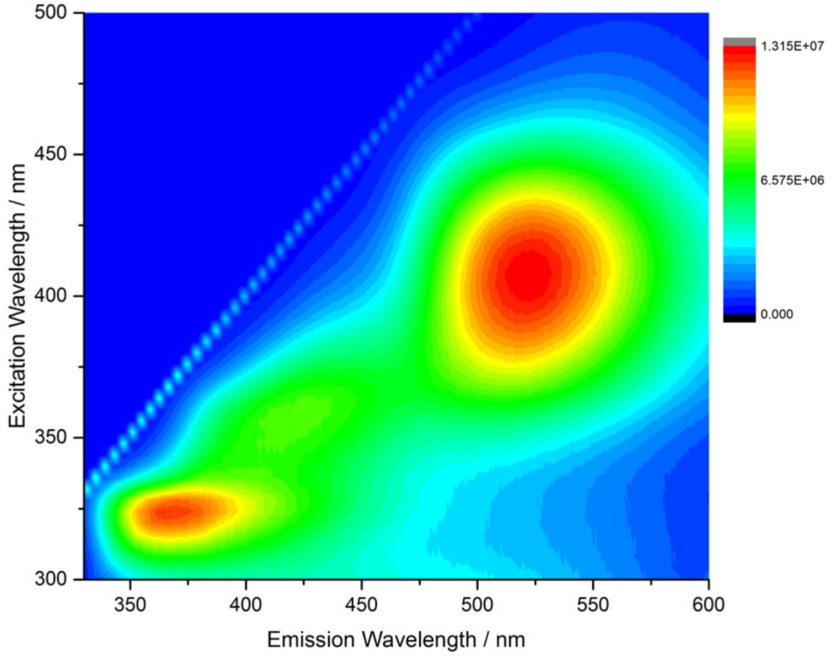

Fig. S4: Excitation/Emission plot of CND1 in water.

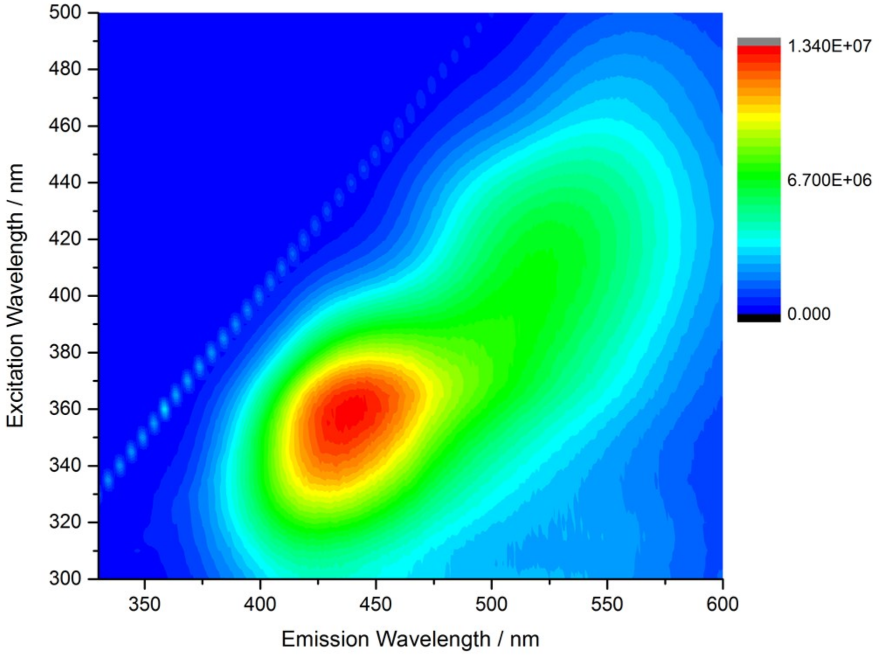

Fig. S5: Excitation/Emission plot of CND2 in water.

Dependence of Solar Cell Performance on Sensitization Time and pH

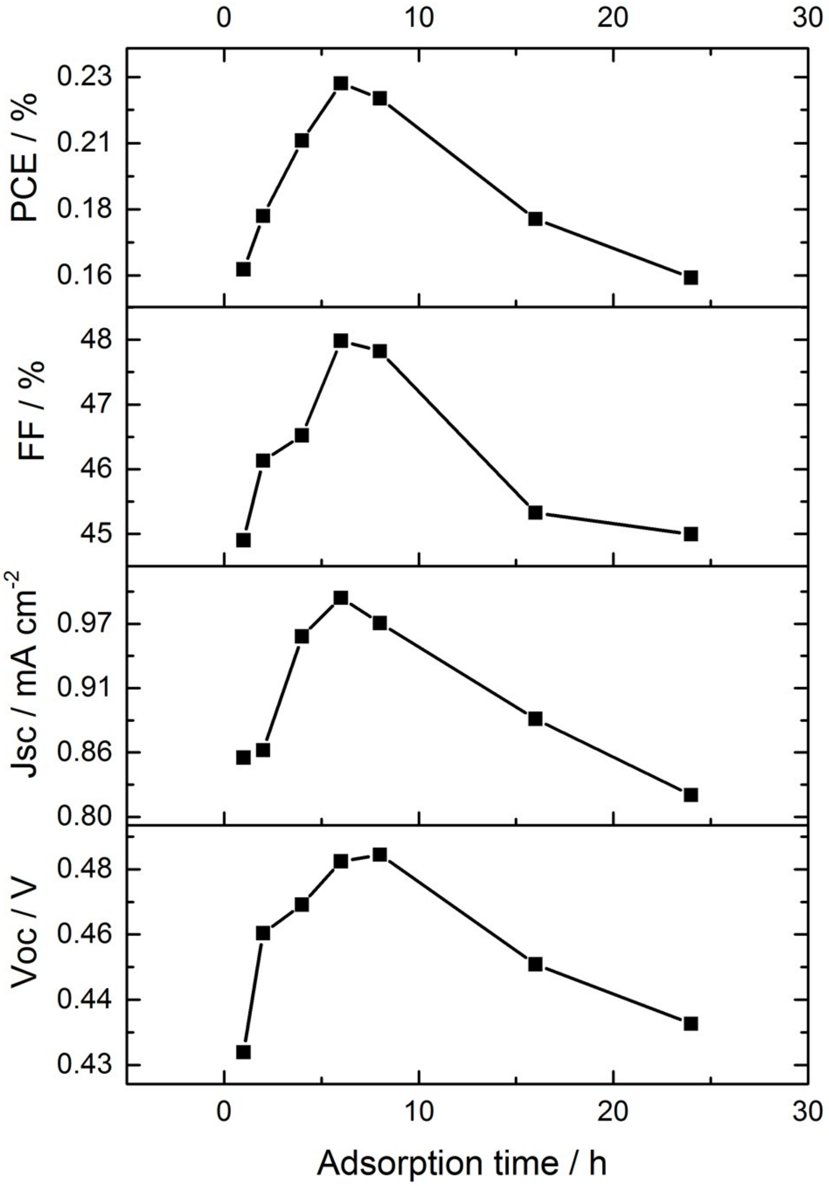

Fig. S6: Dependence of solar cell performance on sensitization time. Solar cell characteristics are averages of two cells sensitized at pH 1.

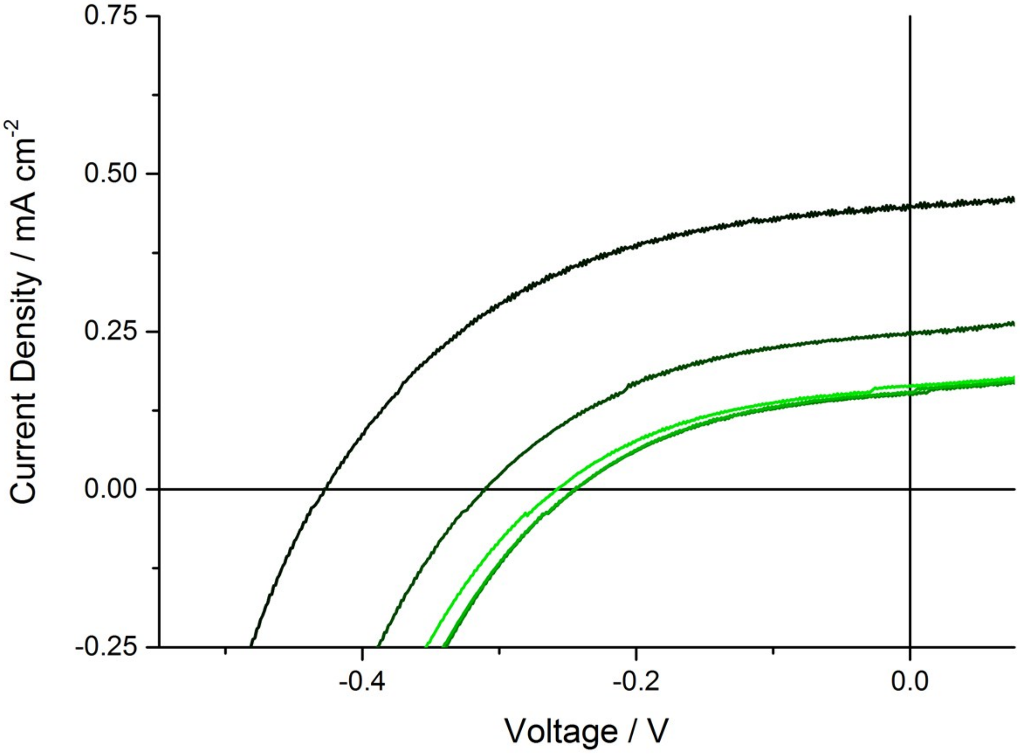

Fig. S7: Dependence of CND1 solar cell performance on pH, using water with pH 7 (light green) to 1 (black) as solvent for sensitization. Sensitization time was 16 h.

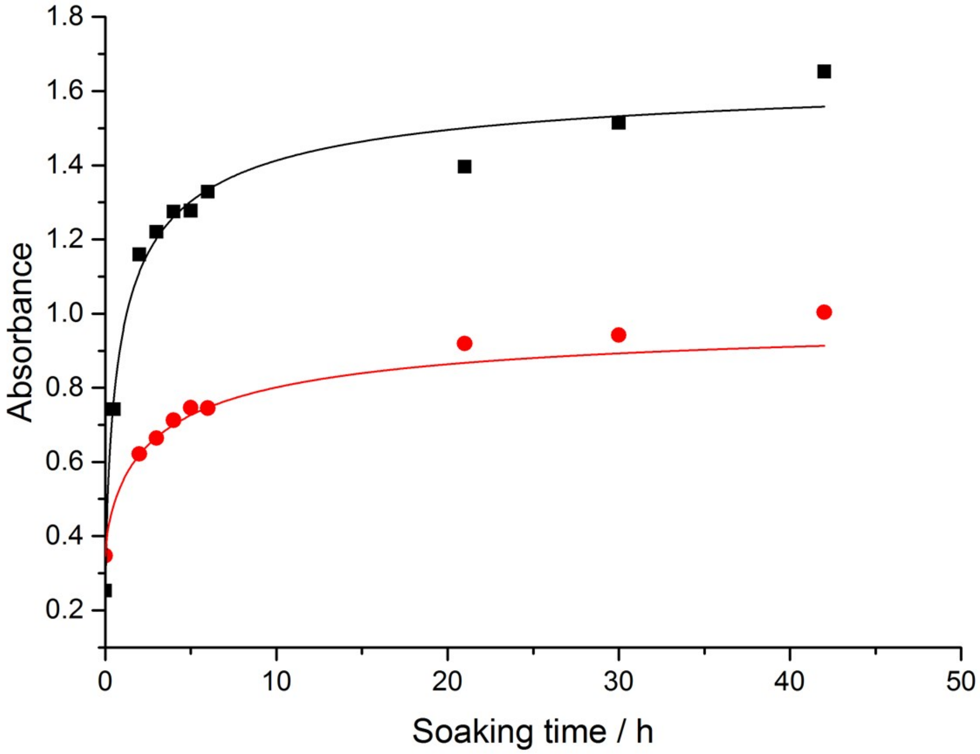

Fig. S8: Absorbance of CND electrodes after different soaking times, measured at 400 nm. Black squares indicate adsorption at pH 1, red circles at pH 7. The lines are a guide for the eye.

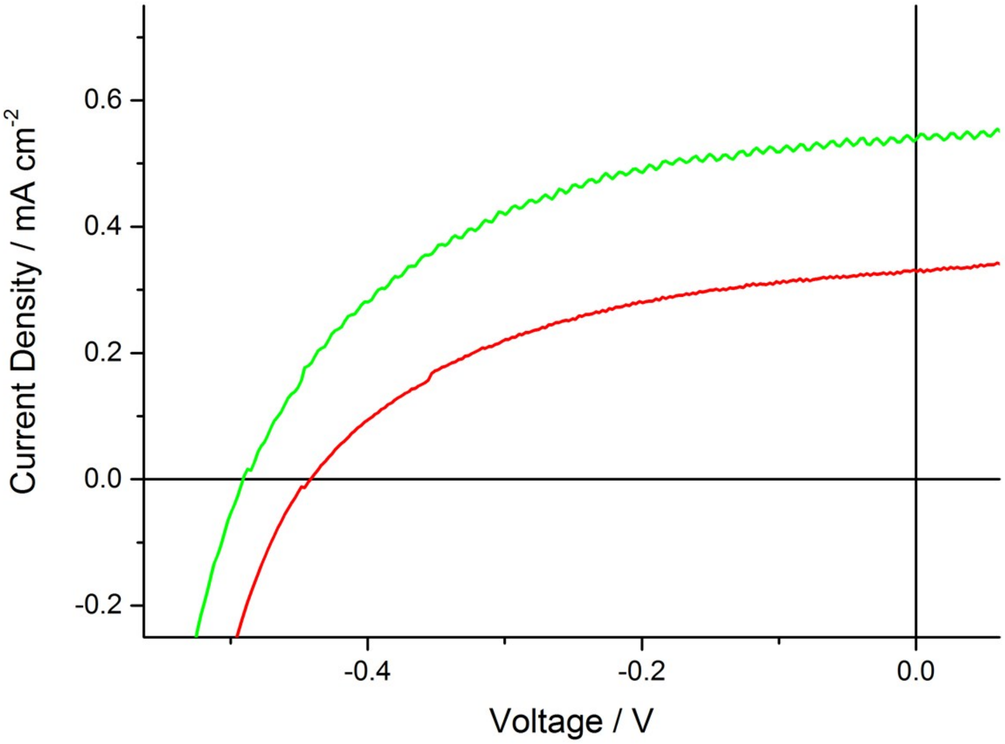

Fig. S9: J-V-curves of solar cells sensitized with CND1 (green) and CND2 (red) (at pH 1 for 16 h).

SEM Microscopy

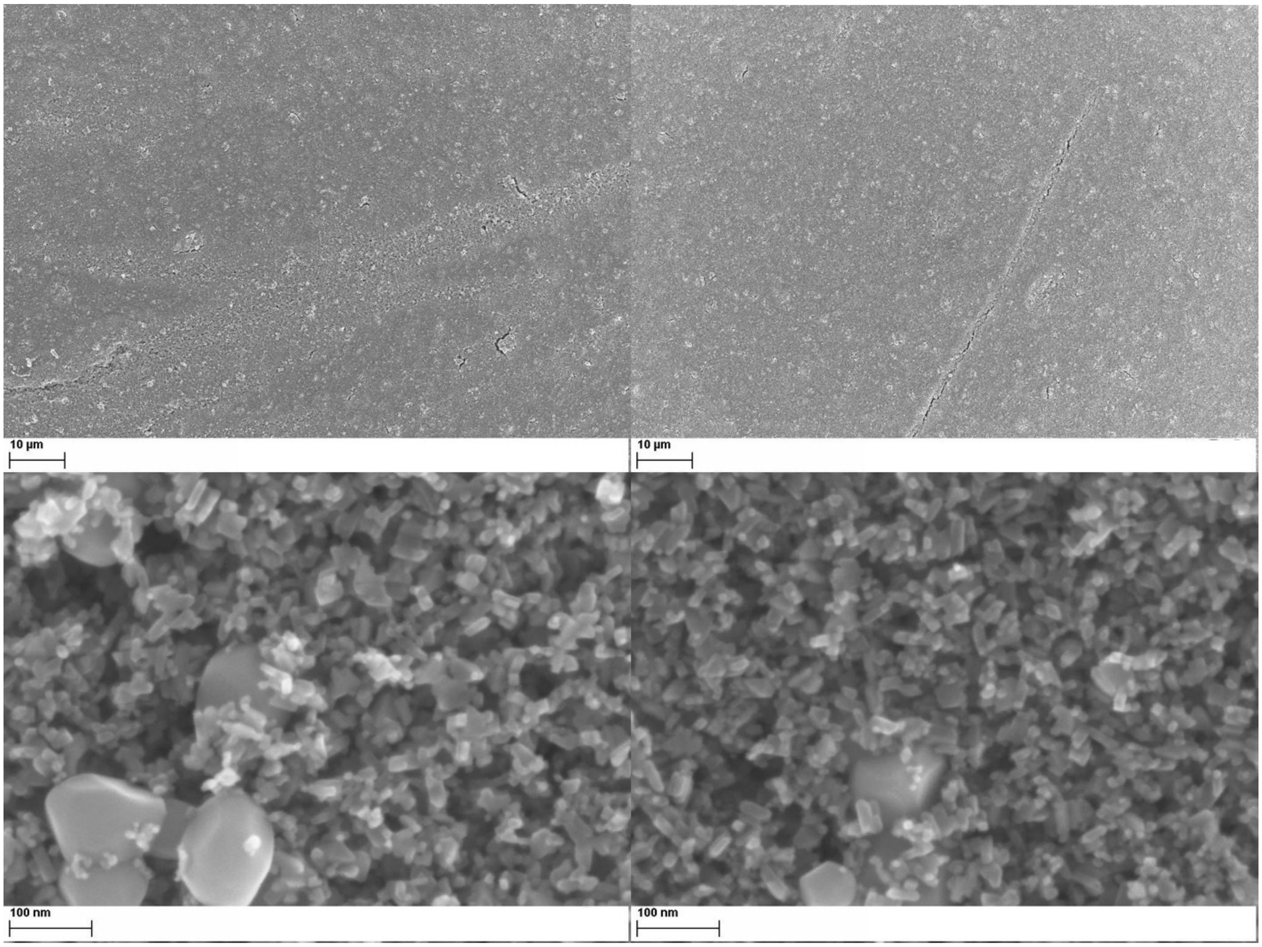

Fig. S10: SEM images of mesoporous TiO_2 electrodes after sensitization at pH 7 (left) and pH 1 (right).

Zeta Potential Measurements

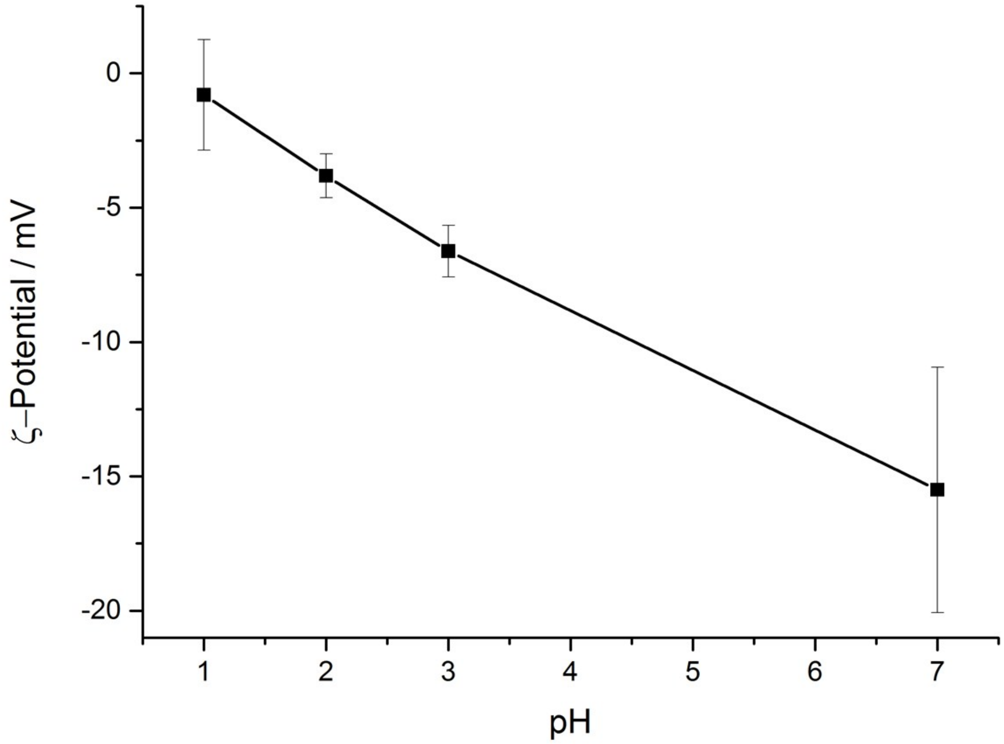

Fig. S11: pH-dependent ζ-Potential of CND1.

Absorption Spectra of CND1 and CND2 sensitized TiO_2 slides

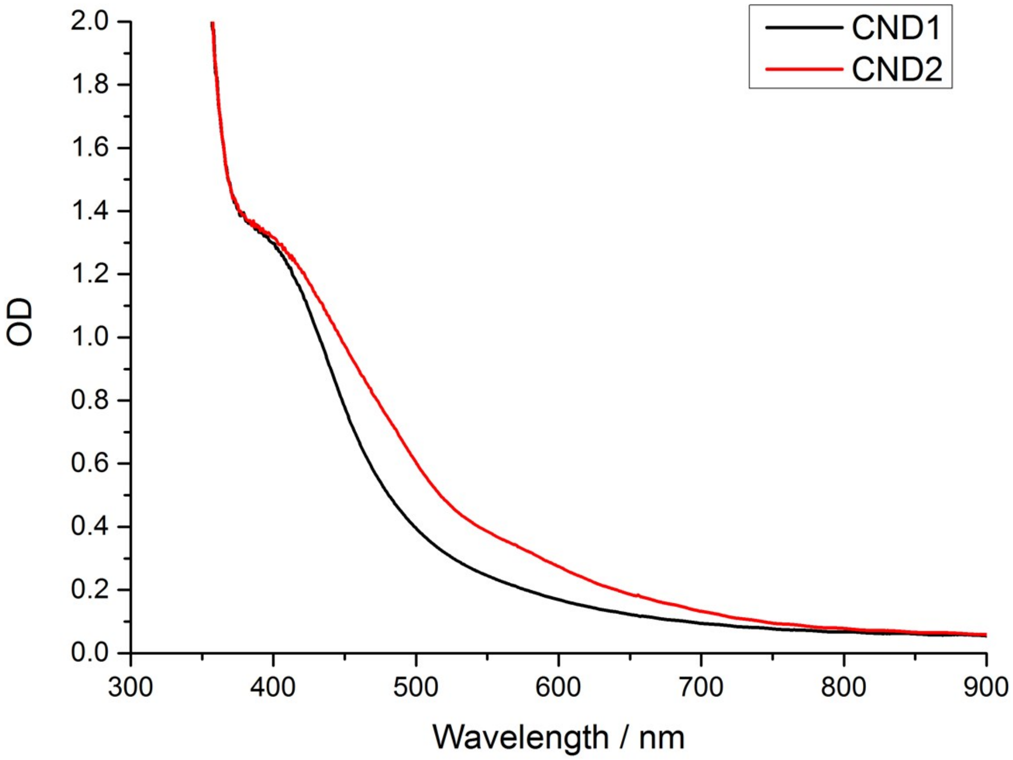

Fig. S12: Absorption spectra of CND1 (black) and CND2 (red) sensitized TiO_2 electrodes.

Femtosecond Transient Absorption Spectroscopy and Time Correlated Single Photon Counting

We conducted femtosecond transient absorption measurements of thin films of **CND1**-sensitized TiO_2 upon excitation at 480 nm. Representative spectra at several time delays between 0 – 7500 ps are shown in Fig. S6. On the blue end of the spectra the ground state bleaching of **CND1** can be seen. The broad positive transient in the region from 550 – 750 nm and its extension in the NIR is attributed to the charge injection into TiO_2. The charge injection is completed within a lifetime of 2.3 ps that was fitted in the bleaching and the injection feature. The long lifetime component of 190 ps in the positive transient at 660 nm is assigned to the charge recombination.[1]

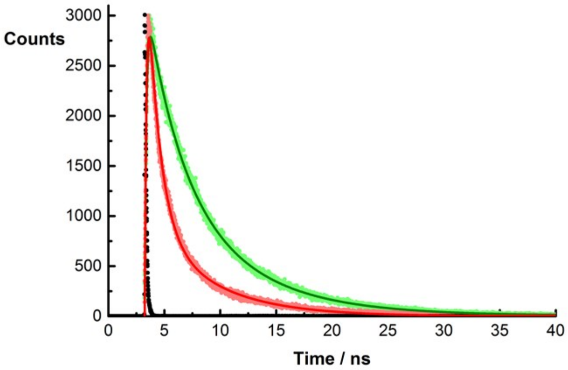

Fig. S13: Emission-time profiles of CND1 at 550 nm obtained by TCSPC upon excitation at 403 nm. The green curve indicates the decay in neutral water, the red curve at pH 1.

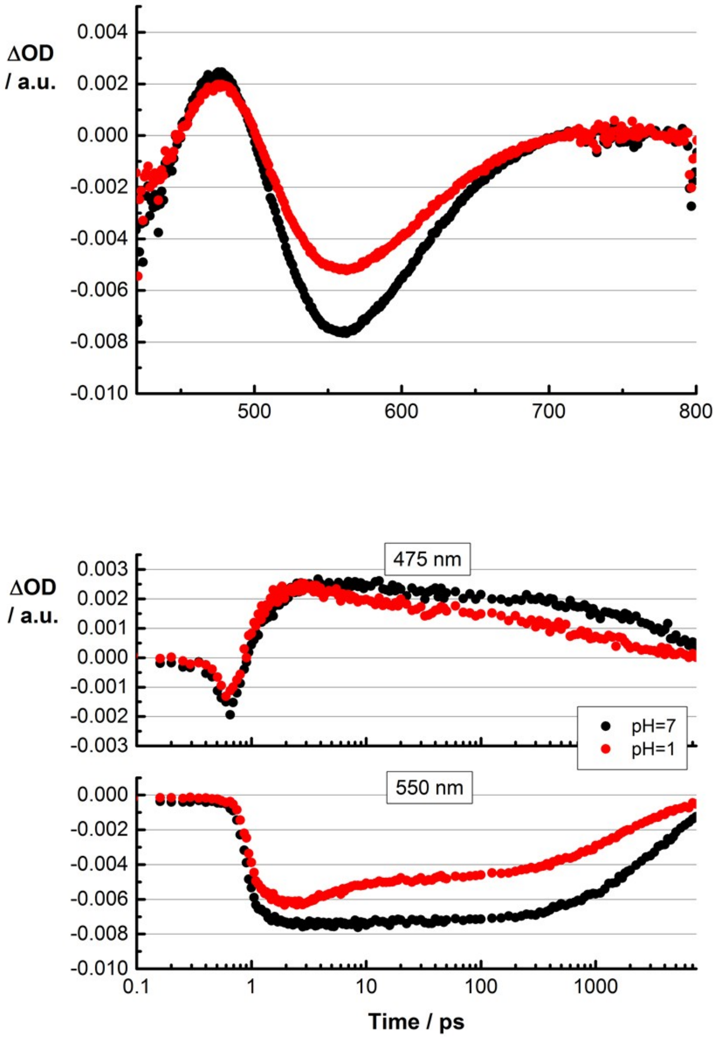

Fig. S14: Above: differential absorption spectra obtained upon femtosecond pump probe experiments (387nm) of CND1 at pH 7 (black) and pH 1 (red) recorded 10 ps after excitation at room temperature. Below: logarithmic time absorption profiles of the spectra shown above at 475 and 550 nm.

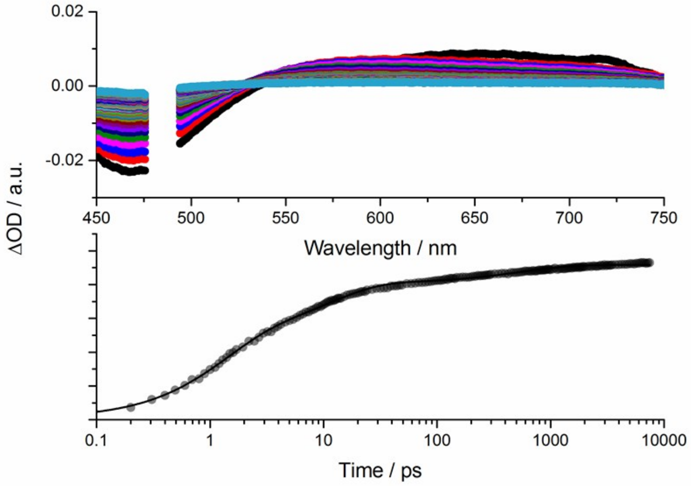

Fig. S15: Above: differential absorption spectra obtained upon femtosecond pump probe experiments (λ_{ex} = 480 nm) on a CND1 sensitized TiO_2 electrode in the presence of acetonitrile with several time delays between 0 and 7500 ps. Below: time absorption profile of the spectra shown in the upper part at 465 nm, monitoring the decay of the CND ground state bleaching.

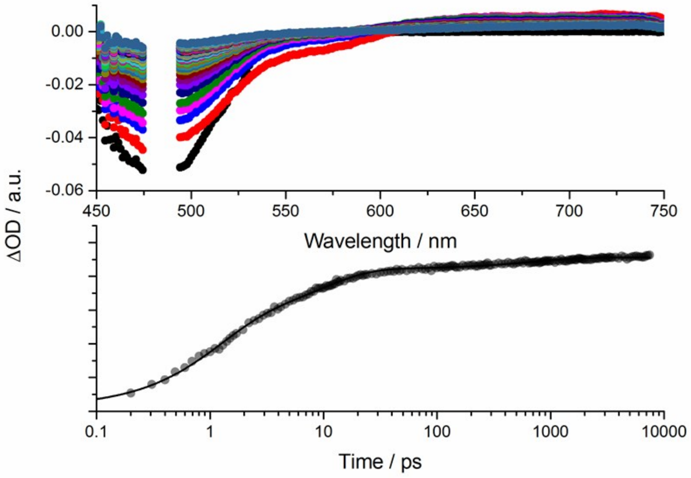

Fig. S16: Above: differential absorption spectra obtained upon femtosecond pump probe experiments (λ_{ex} = 480 nm) on a CND2 sensitized TiO_2 electrode in the presence of I^-/I_3^- electrolyte with several time delays between 0 and 7500 ps. Below: time absorption profile of the spectra shown in the upper part at 465 nm, monitoring the decay of the CND ground state bleaching.

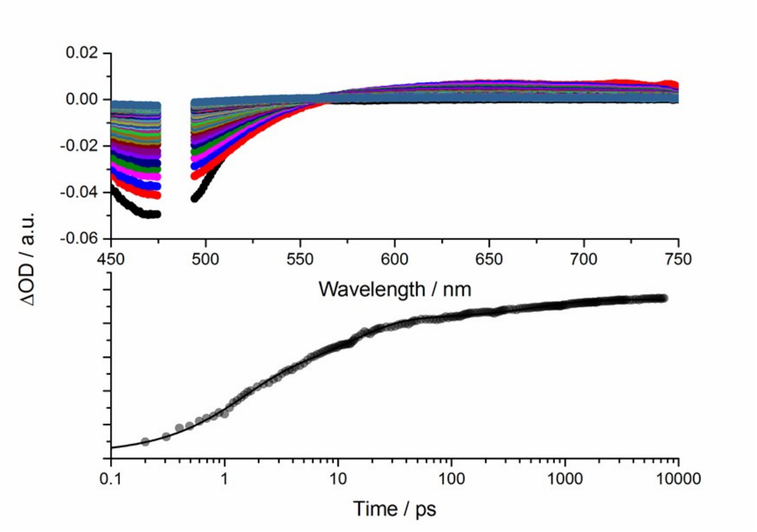

Fig. S17: Above: differential absorption spectra obtained upon femtosecond pump probe experiments (λ_{ex} = 480 nm) on a CND2 sensitized TiO_2 electrode in the presence of acetonitrile with several time delays between 0 and 7500 ps. Below: time absorption profile of the spectra shown in the upper part at 465 nm, monitoring the decay of the CND ground state bleaching.

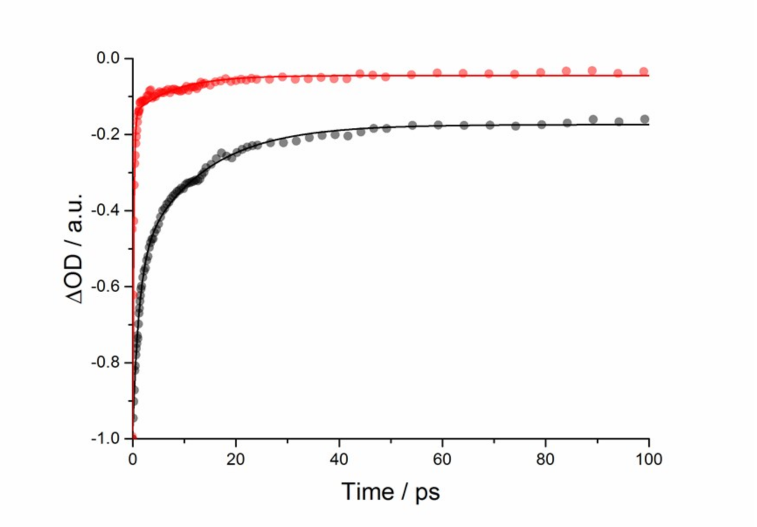

Fig. S18: Time absorption profiles of the spectra shown in the upper part of Fig. S16 at 465 (black) and 550 nm (red), monitoring the decay of the CND ground and trap state bleaching.

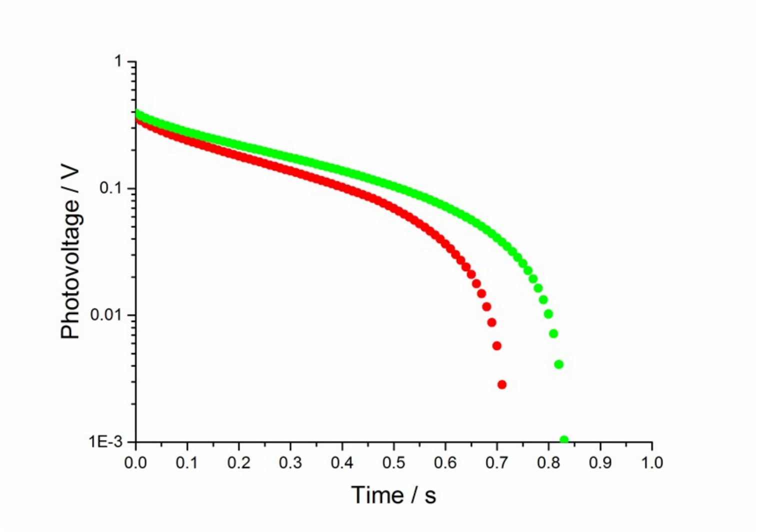

Fig. S19: Photovoltage decay of CND1 (green) and CND2 (red) solar cells.

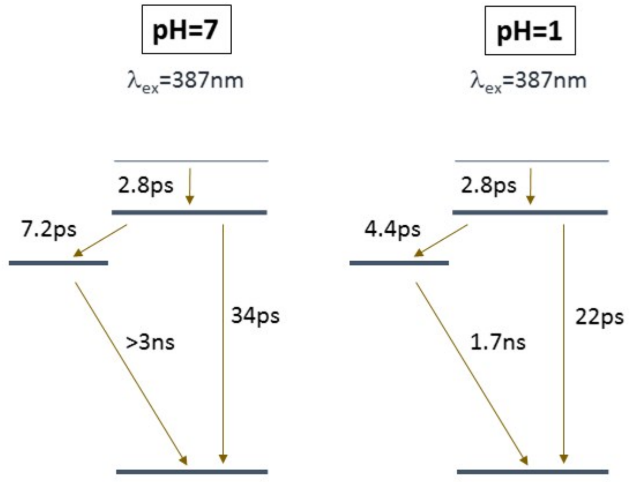

Fig. S20: Schematic energy diagrams of CND1 at pH 7 and pH 1.

---

[1] J. Walter, K. Löhr, E. Karabudak, W. Reis, J. Mikhael, W. Peukert, W. Wohlleben and H. Cölfen, *ACS Nano*, 2014, **8**, 8871-8886.

[2] H. M. Strauss, E. Karabudak, S. Bhattacharyya, A. Kretzschmar, W. Wohlleben and H. Cölfen, *Colloid Polym. Sci.*, 2008, **286**, 121-128.

[3] E. Brookes, W. Cao and B. Demeler, *Eur. Biophys. J.*, 2010, **39**, 405-414.

[4] G. Gorbet, T. Devlin, B. I. Hernandez Uribe, A. K. Demeler, Z. L. Lindsey, S. Ganji, S. Breton, L. Weise-Cross, E. M. Lafer, E. H. Brookes and B. Demeler, *Biophys. J.*, 2014, **106**, 1741-1750.

[5] Hennemann, M.; Clark, T. EMPIRE: A Highly Parallel Semiempirical Molecular Orbital Program: 1: Self-Consistent Field Calculations. *J. Mol. Model.* **2014**, *20*, 2331−2341.

[6] Dewar, M. J. S.; Zoebisch, E. G.; Healy, E. F.; Stewart, J. J. P. Development and Use of Quantum Mechanical Molecular Models. 76. AM1: A New General Purpose Quantum Mechanical Molecular Model. *J. Am. Chem. Soc.* **1985**, *107*, 3902−3909.

[7] Berendsen, H. J. C.; Postma, J. P. M.; van Gunsteren, W. F.; DiNola, A.; Haak, J. R. Molecular-Dynamics with Coupling to an External Bath. *J. Chem. Phys.* **1984**, 81, 3684–3690.